SAND2011-7831P

MEMS Neural Probes

Jit Muthuswamy[1] and Murat Okandan[2]

1 – School of Biological and Health Systems Engineering, Arizona State University, Tempe, AZ 85287-9709

2 - Advanced MEMS and Novel Silicon Technologies, Sandia National Laboratories, Albuquerque, NM, 87185

Sandia National Laboratories is a multi-program laboratory managed and operated by Sandia Corporation, a wholly owned subsidiary of Lockheed Martin Corporation, for the U.S. Department of Energy's National Nuclear Security Administration under contract DE-AC04-94AL85000.

Brain monitoring technologies

Any hypotheses regarding brain function or dysfunction is eventuallyverified and confirmed using accurate measurements of brain activity at different scales– from whole brain regions to single cells or neurons and sub-cellular structures such as synapses, ion channels etc. Such measurements are made using a variety of different techniques each with their ownspatial and temporal resolution. The technologies are generally invasive or non-invasive; the non-invasive technologies include a whole spectrum of imaging modalities as illustrated in Fig. 1, electroencephalograms (EEG) from the scalp, etc.

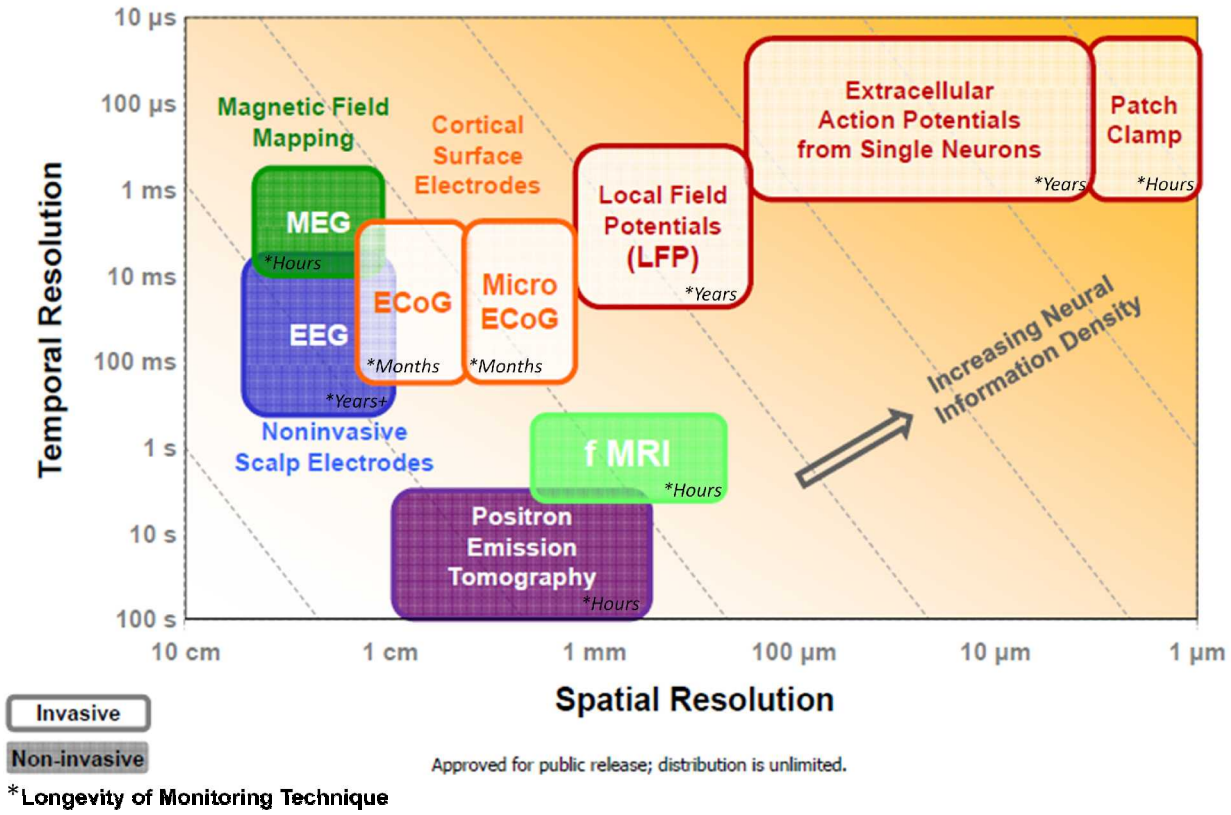

Figure 1. Illustration of the spatio-temporal resolution of current brain monitoring technologies. (courtesy: Jack Judy, program manager, DARPA (MTO), approved for public release; distribution is unlimited)

The invasive technologies typically involve electrodes placed either on the brain (such as in electrocorticogram or ECoG) or microelectrodes implanted in specific brain regions of interest for obtaining electrical activity from the brain in the form of field potentials from ensembles of neurons or extra-cellular action potentials from single neurons or a few neurons in the vicinity of the microelectrode. Generally, electrical activity from single neurons has been a preferred currency for testing hypotheses about brain function. Over the last 10 years, exciting applications such as cortical prostheses have also been developed using electrical activity from single neurons in motor and pre-motor cortices of the brain. Success in this effort will lead to wider application of this theme in other brain prosthetic applications such as memory and cognitive prostheses, etc. While neural probes of all kinds have been developed for other applications such as electrical stimulation of specific neurons in deep brain stimulation (DBS) therapy, monitoring neurotransmitters and other neurochemicals, delivering drugs, micro-electromechanical systems (MEMS) based technologies are currently used in mainstream research and emerging prosthetic technologies primarily for monitoring electrical activity from single neurons. Therefore, this chapter here will focus primarily on neural probes used for monitoring the electrical activity of single neurons.

Implantable technologies to monitor electrical activity from single neurons have been around for over 6 decades now. The earliest single neuronal recordings consisted of manually fabricated glass micropipettes that tapered down to few microns at one end. These pipettes were back filled with electrolytes and a conducting wire was inserted. The tapered end was stereotactically positioned in the brain after a craniotomy in the vicinity of neurons of interest. They were initially used to record intra-cellular membrane potential changes [1-2]. Insulated tungsten or platinum microelectrodes were used for recording extra-cellular activity [3-4]. One of the first attempts to use such cumbersome manual approaches to obtain long-term recordings from awake-behaving animals was Strumwasser's bold efforts in 1958 [5] to record from specific neurons in hibernating California ground squirrels. This era was

then followed by several decades during which bundles of metal microwires in different configuration were manually assembled along with interconnects to record from ensembles of single neurons in the brain. The microwires were insulated along the length and the insulation at the tip of the microelectrode was etched to approximately few tens of microns that will allow successful electrical interface with single neurons in the brain. The size (and consequently the electrical impedance) of the uninsulated tip or the recording site determined the number of neurons that will be recorded by the microelectrode. Microelectrodes developed using MEMS based approaches have been a relatively recent development and have significantly evolved in complexity over the last 25 years. The development of the first neural probe using microfabrication technologies in 1970 [6] demonstrated the promise of MEMS based systems to make neural probes more usable for beginners, dramatically improved consistency in performance, scalability in terms of number of neurons that could be recorded, with a manufacturing process that readily allowed batch-fabrication. MEMS technologies also brought with it the advantage of reliable interconnects that until then was manually soldered or glued and a significant reduction in overall form factor that allowed for animals to behave naturally without any hindrance.

General features of neural probes

The structure of an individual neural probe requires them to be slender (tens to hundreds of micrometers in diameter or in cross-sectional dimensions) and several millimeters long that will allow interrogation of neurons in the cortical and deep brain structures without creating much trauma and displacement of brain tissue during penetration and eventual implantation. Multiple probes are often integrated to form arrays of neural probes. Some studies [7-8] have suggested that slender probes with smaller cross-sectional areas significantly decrease the reactive response of the brain tissue to the foreign body implant. However, the lower limit for slenderness appears to be that which will allow for successful penetration through the superficial meningeal layers of the brain and eventually the brain

tissue itself for accurate placement in the brain region of interest without bending or buckling of the probe. A smooth tapered probe is generally preferred to minimize dimpling of the meningeal layers such as the dura mater during penetration. The likelihood of such tissue dimpling is eventually also dependent on the velocity of penetration and also on the number of such probes constituting an array.

One of the features of a probe used for recording from single neurons are the presence of one or more recording sites along the length of a probe. To ensure recording from one neuron or a few selective neurons, the recording sites are of similar geometrical scale as the neuronal cell bodies (which are typically 10-20 μm in diameter in the mammalian brain). Ion-exchange across the cell membrane during a neuronal action potential results in current flow. The current flow in a volume conductor results in lines of electrical field intensities and spatial potential gradients being established in the extra-cellular space. Microelectrodes in the extra-cellular space therefore register the spatial potentials (typically less than 1 mV) at any given point. The interface between the recording site (typically made of metals like platinum, platinum/iridium, gold and also sometimes doped polysilicon) and the surrounding ion-rich extra-cellular media usually determines the overall electrical impedance of the probe with respect to a reference electrode typically placed at a distance from the recording microelectrode (on/in the brain, or on the neck muscles depending on the application and the type of recording desired). The recording interface itself is largely capacitive due to the spontaneous formation of a double layer of ions on the surface of the recording site of the probe immediately upon insertion into the ion-rich media. However, faradaic reactions that take place at the recording site give rise to a parallel pathway for charge transfer between the recording site and the surrounding ion-rich media that can be modeled as a resistive pathway in parallel to the double-layer capacitance.

Given the above general mechanical and electrical features of neural probes, two broad classes of MEMS micromachining techniques namely, bulk micromachining and surface micromachining have been used successfully to fabricate slender neural probes and arrays of neural probes out of silicon

wafers. Silicon has generally been a preferred substrate material for a variety of reasons. Well established micromachining methods, tools and recipes are readily available. Further, silicon lends itself readily to subsequent integration of circuitry and other functionalities. Silicon has also been shown to be non-reactive or inert as an implant material [9] that elicits minimal foreign body response. Directional, material and dopant dependent selectivity of anisotropic etching is used in both of the above techniques to machine microscale mechanical structures in the form of slender neural probes. In addition to the above two, MEMS neural probes have also been fabricated out of polymers spun-coat on micromachined silicon or metal molds. A wide variety of MEMS neural probes have been developed and tested, but only a few representative technologies that are broadly distinct in their approaches and have been tested in long-term animal experiments are described here.

Bulk micromachining of MEMS neural probes

The first MEMS based neural probes were micro-scale shanks of silicon with metal recording sites along the length [10]. They were fabricated by bulk micromachining of silicon using anisotropic etching techniques. A boron dope silicon substrate acted as an etch-stop and shanks of silicon 8-15 μm in thickness, 75-100 μm in width at the base that narrowed down to 25 μm and 1.5-3 mm length were machined in the initial versions. Each shank was capable of hosting multiple recording sites of gold with polysilicon or tantalum conductors. Currently these probes are fabricated and distributed by Neuronexus Inc., Ann Arbor, MI.

Another widely used silicon MEMS technology using bulk micromachining is a 3-D array of 10x10 microelectrodes (total of 100 microelectrodes) that was first reported in 1991 from University of Utah [11]. Aluminum (5 μm thick) was deposited on the polished surface of silicon wafers (1.7 mm thick) and then patterned into squares (325 μm sides and 400 μm separation between the centers of adjacent squares). A temperature gradient between the two sides of the wafers created a thermal migration of the eutectic of droplets of aluminum and silicon with silicon recrystallizing behind the trail of eutectic droplets. The

net result was the creation of highly conductive trails of doped (p+) silicon within the bulk silicon wafer. Chemical and mechanical polishing of the wafer resulted in pillars of p+ doped silicon (approximately 1.5 mm long) isolated from its immediate neighbors by back-to-back p-n junctions that provided the isolation. The pillars were finally coated with platinum at the tip and insulated with polyimide after establishing interconnects at the back end. Bulk micromachining approaches have also been used successfully with other materials such as ceramic and diamond.

Surface micromachining of MEMS neural probes

Surface micromachining allows the fabrication of neural probes that are generally thinner (2-5 μm thick) than typical bulk micromachined probes (>8-15 μm thick). There is no evidence yet that a reduction in one of the dimensions of the neural probes leads to an improvement in performance. However, a significant reduction in the cross-sectional area of the neural probe has been shown to significantly improve the inflammatory and foreign body reaction of the tissue immediately surrounding the neural probe [7-8]. There are other significant and unique advantages of surface micromachining over bulk micromachining such as the ability to integrate (a) complex mechanical structures such as microactuators, gears etc. on the same die (b) signal conditioning and control circuitry to significantly enhance the functionality of neural probes.

One such area where complex mechanical structures such as microactuators and gears can potentially enhance the reliability and functionality of the neural probe is in the development of autonomous neural probes that are capable of adapting their position in the brain to compensate for any change in the quality of neuronal signal being recorded [12]. Such movable neural probes enhance our ability to (a) obtain well isolated and stable single neuronal activity with high signal-to-noise ratio over longer durations and also to carefully and unambiguously monitor changes in the underlying neurobiology (b) monitor neurons and neuronal tracts of specific functional interest (c) potentially

enhance the reliability of brain prosthetic devices that require reliable operation over a life-time of the patient.

Innovative approaches have been used to develop neural probes using surface micromachining process. One such approach for developing a 3D-array of neural probes involved the fabrication of polyimide pillars (1.5 mm long) with metal (Titanium on Aluminum) traces for 3 recording sites on each pillar, as opposed to the single recording site that was found in the Utah microelectrode array [13]. Polyimide film (10 μm) was spun coat over a 5 μm thick film of Nickel electrodeposited on silicon. Nickel acted as a backing metal for the polyimide film. After patterning the metal interconnects and recording sites on the polyimide film, a second layer of polyimide (also 10 μm) was spun coat on top. Finally, and most interestingly, an externally applied magnetic field was used to lift the Nickel backing layer and along with it the polyimide films that sandwich the metal interconnects and recording sites. Similar surface micromachining approaches have been used to fabricate slender neural probes from other polymers such as benzocyclobutene (BCB).

One of the key challenges in using surface micromachining approaches to fabricate neural probes is to ensure no residual stress in the thin films that constitute the substrate of the neural probe. Simultanesously, the thin films will also need sufficient stiffness to penetrate the outer meningeal layers and the brain itself and travel through the brain tissue without significant bending, buckling or breaking. The five-layer polysilicon SUMMiTV^{TM} (Sandia's ultra-planar multi-layer micromachining technology) process of Sandia National laboratories, Albuquerque, NM has been extremely useful in fabricating complex, surface micromachined, movable neural probes that have been tested successfully in long-term animal experiments. Details of this process are explained in the remaining sections of this essay.

SUMMiT^{TM} Surface Micromachining Process

A condensed process flow of the key process steps for an example rotating gear element

encapsulated by the uppermost layer of polysilicon is shown in Fig. 2a-j. The polysilicon layers are denoted P0, P1, P2, P3, and P4, where P0 is a non-construction layer used primarily for electrical interconnect and as a ground plane, and P1 to P4 are the mechanical construction layers. All polysilicon films are deposited as n-type, fine-grained polysilicon from silane in a low pressure chemical vapor deposition (LPCVD) furnace. Similarly, the intervening sacrificial oxide layers are denoted as S1, S2, S3, and S4, where S1 resides between P0 and P1, S2 between P1 and P2, and so forth. Except for the backfill oxide used prior to CMP planarization, the oxide films are also deposited in an LPCVD furnace. 150mm, (100) n-type silicon wafers of 2 to 20 ohm-cm resistivity are used as the substrate, from which an oxide is thermally grown followed by a low-stress LPCVD silicon nitride film of 8000 Å thickness [14]. The dielectric layers of low-stress silicon nitride and thermal oxide are on the substrate for electrical isolation. The exact composition and construction of the dielectric isolation films added to the silicon surface are not critical, but they must provide electrical isolation between the substrate and separate devices, survive the release etch, and have limited impact on mechanical stresses in the substrate.

If desired, these dielectric films can be patterned and etched to provide vias for electrical contact to the substrate, for example, to provide a uniform ground plane. The electrical interconnect layer, P0, is next deposited as an in situ, phosphorus-doped LPCVD polysilicon film of 3000Å thickness. The film is photolithographically patterned and reactive ion plasma etched (RIE) for interconnect/electrode geometry. The first layer of sacrificial oxide, S1, is deposited by LPCVD to a thickness of 2 μm. This film receives two definition and etch steps to produce dimple and anchor points. The dimples produce physical standoffs to limit vertical contact of P1 to the substrate, serving to reduce in-use adhesion of the P1 layer to the substrate. The anchor points provide an area cut through the S1 layer to allow subsequent polysilicon layers to be attached both mechanically and electrically to the underlying P0 layer, in this case, the central hub of the example gear. The oxide etch is designed to rapidly etch the oxide film with a high selectivity to the underlying P0 film. The device cross section to this point is shown in Fig. 2b.

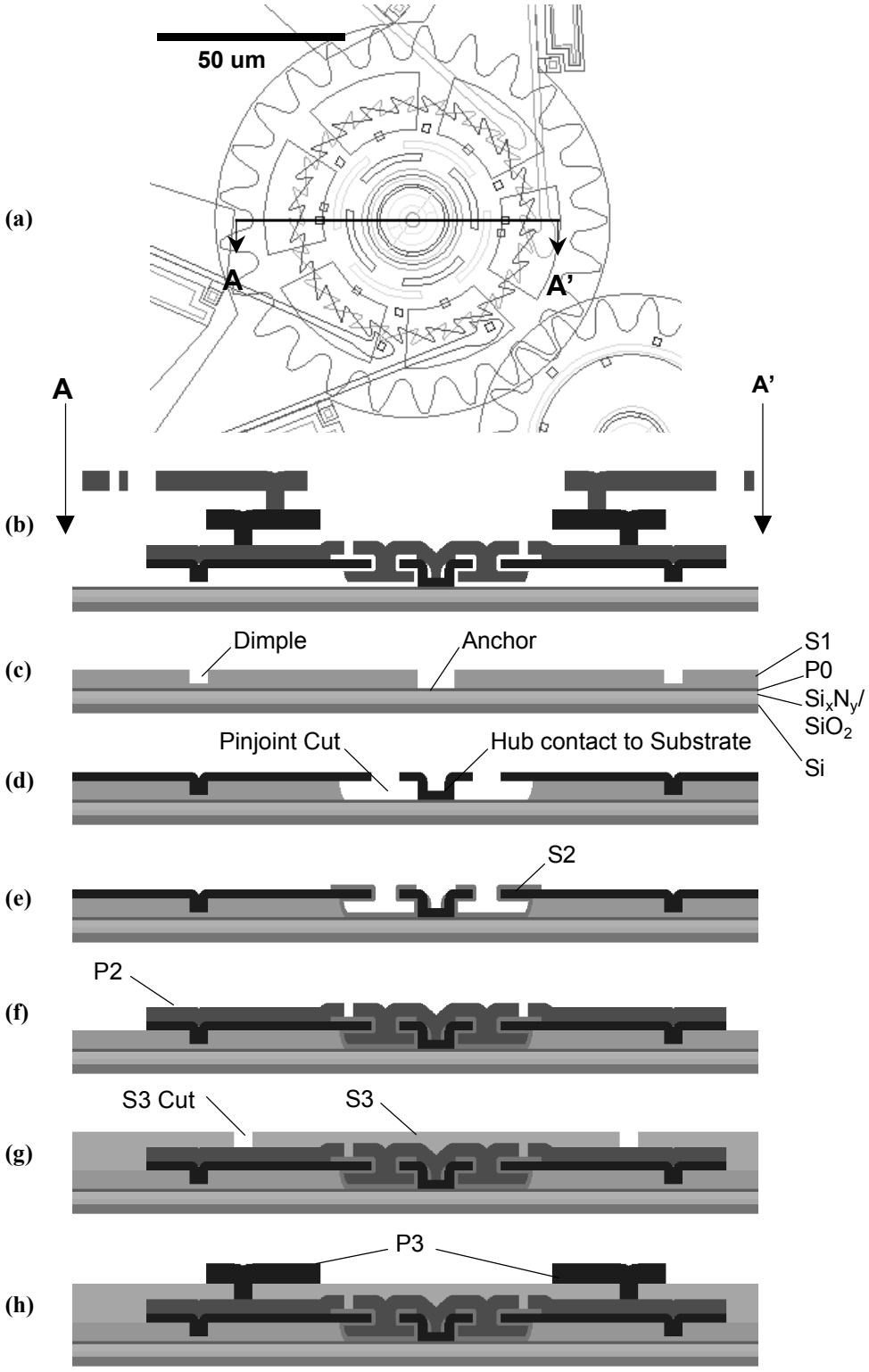

Figure 2. Plan view and cross section of example rotary device illustrating the process technology sequence for fabriaction.

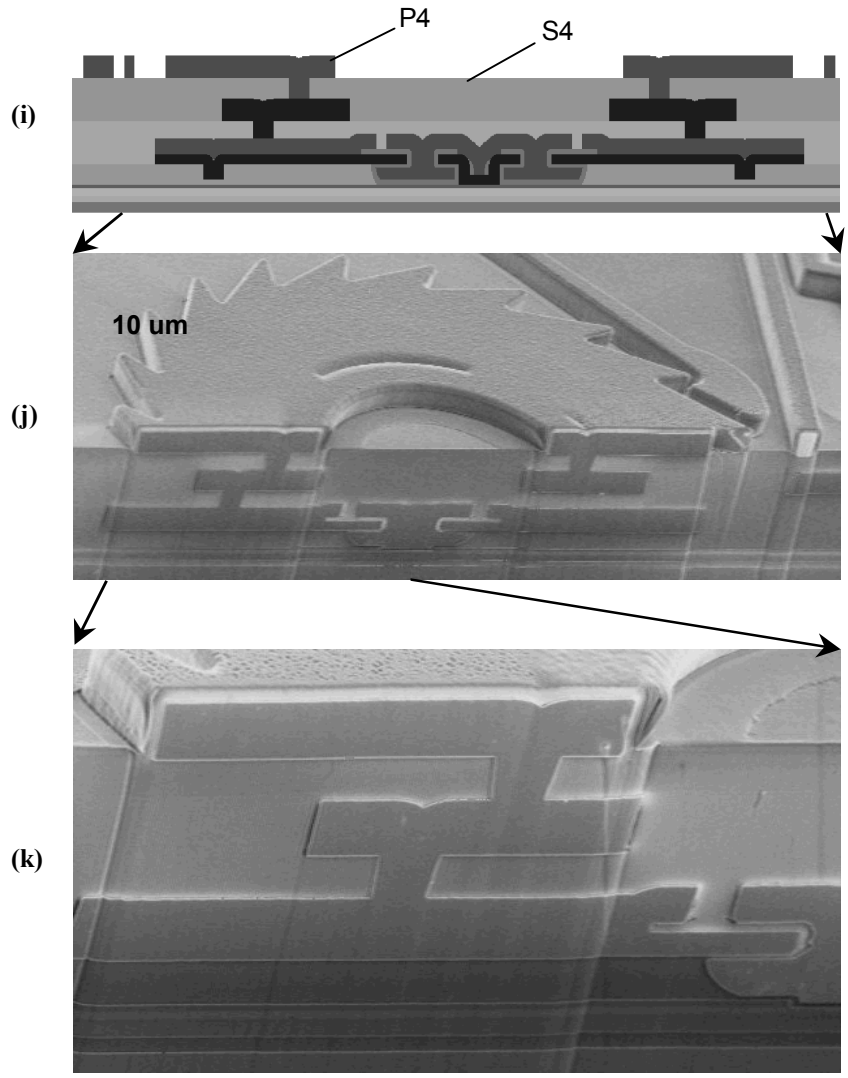

Figure 2 (i-k)

At this point, the first mechanical construction layer, P1, is deposited to a thickness of 1.0μm. In the areas that define the rotary pin or the central hub, the P1 layer is defined with a simple circular hole or an annular ring, respectively. These removed areas of P1 allow an aqueous HF etchant to slightly undercut the P1 layer by isotropically etching the oxide, as shown in Fig. 2c. This begins formation of a simple bushing-type bearing between the central hub (shaft) and the gear. This bearing allows the gear to rotate about the hub, and the pin to rotate in the gear. This approach is an adaptation of the early work by Fan et al. [15] for fabricating bearing structures in polysilicon surface micromachining.

In Fig. 2d, the sacrificial oxide layer, S2, is deposited (0.5μm), patterned, and etched. LPCVD oxide films are conformal in nature. In the context of micromachining, conformality includes the ability of a film deposition to coat areas that have overhangs with undercut recesses in addition to the top and sidewall surfaces of typical interest in IC fabrication. The deposit coats the undercut areas to approximately one-half the nominal deposition thickness on the top surfaces.

The second layer of construction polysilicon, P2, is deposited at a thickness of 1.5 μm. Low pressure chemical vapor deposition (LPCVD) polysilicon is a highly conformal deposition; thus the deposition into the undercut region completely fills this region with a uniform thickness of polysilicon. The polysilicon is patterned and etched, effectively producing solid hub and pin joints as shown in Fig. 2e. The reactive ion etch (RIE) can be used to define only the P2 layer, as shown in the central hub and pin joint area, or it can be used to define the composite film of P1 + P2, as shown in the area that defines the gear and link elements. Here, the RIE selectivity is designed such that the exposed polysilicon is removed at a much higher rate than the underlying oxide.

At this point in the process, the topography on the wafer surface is substantial relative to standard IC photolithographic patterning and etch techniques. In this example, 4.8 μm of topography is generated. To remove this topography, the surface is coated with a thick oxide film (Fig. 2f), followed by a chemical mechanical polishing (CMP) planarization step. The result, after patterning the planarized oxide with an anchor pattern for subsequent attachment of P3, is shown in Fig. 2g. The surface once again is flat, thereby enabling further processing. The third polysilicon, P3, is deposited, patterned, and etched as shown in Fig.2h to produce the interlinking mechanical elements.

Once again, the topography is quite severe, and a second CMP planarization is completed by repeating the procedure for S3 and P3 before deposition of the final polysilicon layer, P4. The final, oxide encased structure is shown in Fig.2i. The final step in the process, referred to as the release step, is to remove all exposed silicon

dioxide sacrificial film with either an aqueous or vapor isotropic HF-based etch [16]. This etchant removes all exposed oxide, including the oxide under or between polysilicon layers, such as S2 in the hub region. Techniques can be used to eliminate release stiction [17-18], but a free-standing device may have contacting/sliding surfaces by design A cross-section of a device designed for the five-level process clearly depicts all levels and illustrates planarization by CMP of the oxide levels prior to deposition of the polysilicon levels four and five (Fig.2j). The total stack height of the dielectric layers is 12.5 µm, and the largest device thickness that can be produced is 12.0 µm. In contrast, single-level processes normally consist of polysilicon film thickness on the order of 2 µm. Thus, the stack is roughly a factor of 6 thicker which, from simple elastic beam theory, implies roughly a cubic increase in out-of-plane stiffness, i.e., a factor of 216 increase in out-of-plane stiffness. This has significant impact on device reliability and operation as it reduces undesired contact of the structures to the substrate, and it reduces out-of-plane deformation due to residual stress gradients in the films. The former can lead to adhesion of the structure to the substrate, while the latter may compromise device design.

The neural probe in the form of a long, slender beam of doped ($10^{21}/cm^3$) polysilicon 7 mm long, 50 µm wide and approximately 5 µm thick is defined in the P 2, P3 and P4 layers of the SuMMITV™ process. Interestingly, the non-linear I-V characteristics of doped polysilicon has an inflection point approximately at the same voltage that typically separates noise signal amplitudes (10-30 µV peak-to-peak) from action-potential signal amplitudes (typically >100 µV) [19]. The above property, remarkably, results in selective suppression of noise when recording extra-cellular potentials from the brain [19]. The polysilicon neural probe has been demonstrated to produce significantly higher signal-to-noise ratios compared to commonly used tungsten neural probes.

MEMS neural probes with electrostatic microactuators

Integrated electrostatic microactuators have been developed for moving neural probes in the brain using comb-drives. Electrostatic forces due to a fringing electric field between a movable plate and stationary plate upon application of a voltage (90-110V) between the two plates creates a movement in one of the plates. A bank of such parallel plates forming a comb drive is used to create translation (~30-40 µm) in the x-direction as shown in Fig. 3.

Figure 3. Schematic of the comb drive actuator and a close-up of one of the parallel plates and the associated fringe field intensity lines that make up the comb drive.

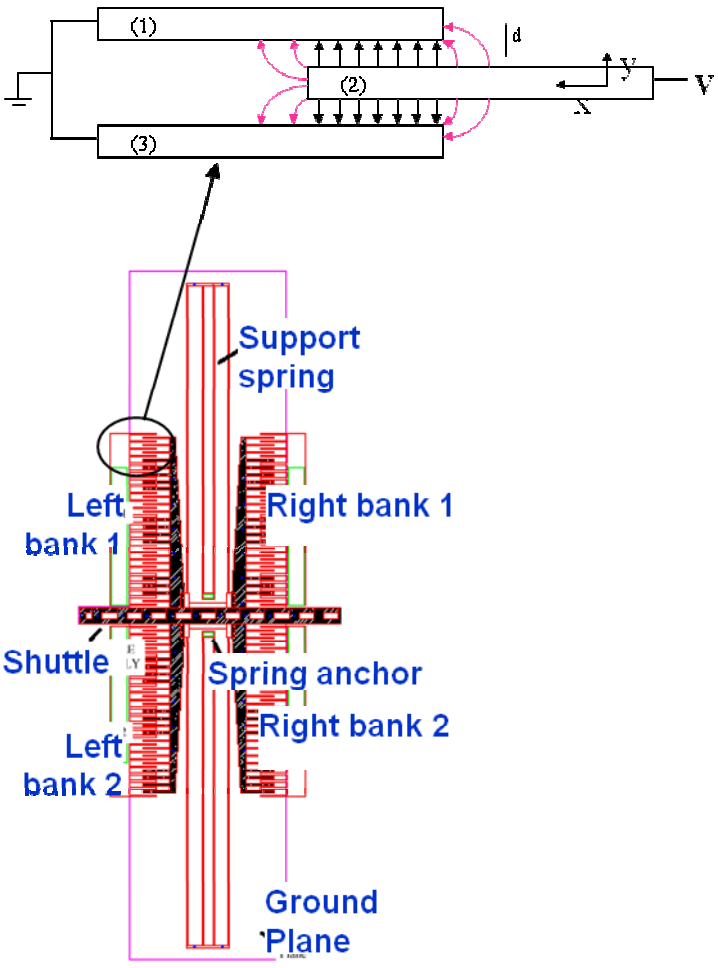

A similar arrangement is used to create translation in the y-direction. The above two systems are driven by voltages that are 90° phase shifted and the translations are coupled to a pin-joint that rotates a fly-wheel as shown in Fig. 4. The direction of rotation of the fly-wheel is determined by which of the two drives (x- or y-drive) is leading in phase. The flywheel is coupled to the microelectrode either directly or through gears to move the microelectrodes in steps of 1 µm over a distance of 5 mm. The above system of electrostatically actuated microelectrodes has been successfully tested in acute rodent experiments [20] but was found to be prone to mechanical failure.

There were stiction issues between the parallel plates of the comb-drive, alignment issues between the gears and the microelectrode that resulted in the microelectrode getting stuck particularly during intense behavioral routines of the rodent. Besides such serious mechanical robustness issue, the electrostatic microactuators also required high voltages (90-110V) and optimally designed voltage waveform shapes.

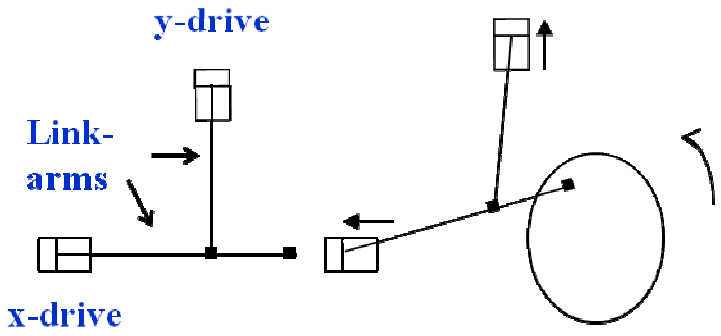

Figure 4. Schematic of the x- and y-drive connected to a pin joint and a fly-wheel. The x- and y-drives are activated at 90° phase difference to produce a net rotational motion of the fly-wheel that will eventually drive a gear or the microelectrode.

Electrothermal microactuators have, on the other hand, been demonstrated to be more robust and occupy smaller footprint on the die [21-22]. In addition, the waveforms required to drive the electrothermal actuators are 6-10V and standard rectangular pulses that can be readily generated. At the core of electrothermal microactuators are the electrothermal strips that consist of parallel beams of doped polysilicon that expand upon the application of voltage, displacing a shuttle in themiddle of the electrothermal strips as illustrated in Fig. 5. Each microelectrode was designed with one set of actuators to move the microelectrode up, one set to move the microelectrode down, two sets of microactuators to release the lock that prevents the microelectrode from moving up, and finally two sets of microactuators to release the lock that prevents the microelectrode from moving down.The above

neural probes had a displacement resolution of approximately 9 μm over a total displacement capability of over 5 mm. The electrothermal microactuators and the integrated neural probes have been successfully tested in long-term rodent experiments lasting over 13 weeks [21].

However, the key challenge in the application of MEMS neural probes in brain prosthetic technologies as well technologies to monitor single neurons for neurobiological applications has been the unreliable interface between the implanted microelectrode and the neurons in the brain tissue surrounding the microelectrode. Current technologies do not have the stability, consistency or reliability to record from targeted single neurons for long periods of time. The MEMS based movable microelectrodes with their flexibility to be repositioned offer a very promising approach to overcome the above challenges.

Figure 5. (a) Schematic of a microelectrode and 6 electrothermal actuators associated with the microelectrode. The 'Up' and 'Down' actuators move the microelectrode in the center up or down respectively. (b) SEM of the one of the actuators showing the electrothermal heat strips and ratchets that move the microelectrode.

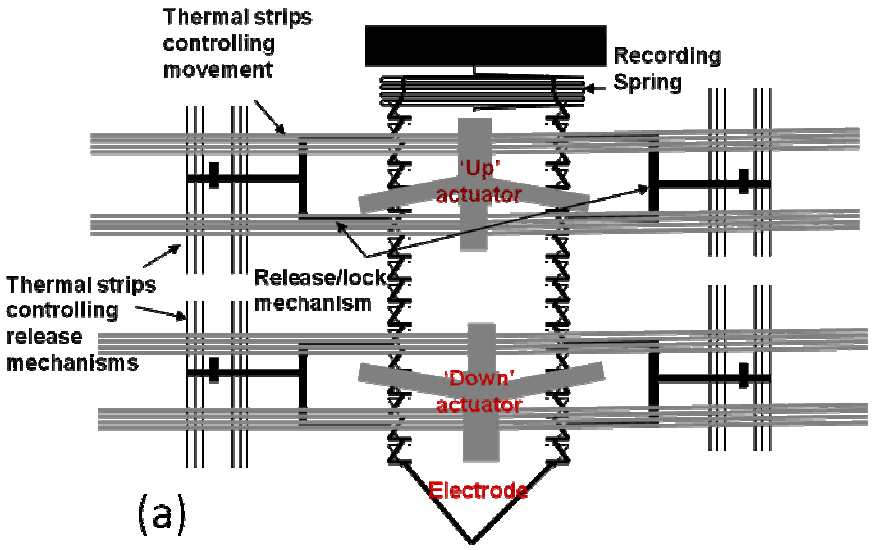

(a)

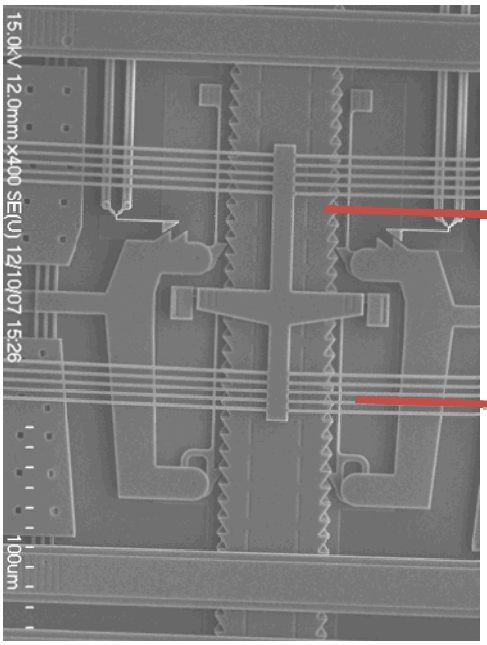

Microelectrode

'Down' actuator

(b)

References

1. K. S. Cole and H. J. Curtis, *J Gen Phys*, 1939, **22**, 649-670.
2. G. Ling and R. W. Gerard, *J Cell Comp Phys*, 1949, **34**, 383-396.
3. R. M. Dowben and J. E. Rose, *Science*, 1953, **118**, 22-24.
4. D. H. Hubel, *Science*, 1957, **125**, 549-550.
5. F. Strumwasser, *Science*, 1958, **127**, 469-470.
6. K. D. Wise, J. B. Angell and A. Starr, *IEEE Trans Biomed Eng*, 1970, **17**, 238-247.
7. J. P. Seymour and D. R. Kipke, *Biomaterials*, 2007, **28**, 3594-3607.
8. P. Stice, A. Gilletti, A. Panitch and J. Muthuswamy, *J Neural Eng*, 2007, **4**, 42-53.
9. S. S. Stensaas and L. J. Stensaas, *Acta Neuropathol*, 1978, **41**, 145-155.
10. K. Najafi, K. D. Wise and T. Mochizuki, *IEEE Trans Electron Dev*, 1985, **ED-32**, 1206-1211.
11. P. K. Campbell, K. E. Jones, R. J. Huber, K. W. Horch and R. A. Normann, *IEEE Trans Biomed Eng*, 1991, **38**, 758-768.
12. J. Muthuswamy, S. Anand and A. Sridharan, *Front Neurosci*, 2011, **5**, 94.
13. S. Takeuchi, T. Suzuki, K. Mabuchi and H. Fujita, *J Micromech Microeng*, 2004, **14**, 104-107.
14. S. Habermehl, *J Appl Phys*, 1998, **83**.
15. L. S. Fan, Y. C. Tai and R. S. Muller, *IEEE Trans Electron Dev*, 1988, **35**, 724-730.
16. Y.-I. Lee, K.-H. Park, J. Lee, C.-S. Lee, H. J. Yoo, C.-J. Kim and Y.-S. Yoon, *J Microelectromech Syst*, 1997, **6**, 226-233.
17. G. T. Mulhern, D. S. Soane and R. T. Howe, Supercritical carbon dioxide drying of microstructures, Yokohama, Japan, 1993.
18. U. Srinivasan, M. R. Houston, R. T. Howe and R. Maboudian, *J Microelectromech Syst*, 1998, **7**, 252-260.
19. R. Saha, N. Jackson, C. Patel and J. Muthuswamy, *IEEE Trans Neural Syst Rehabil Eng*, 2010, **18**, 489-497.
20. J. Muthuswamy, M. Okandan, T. Jain and A. Gilletti, *IEEE Trans Biomed Eng*, 2005, **52**, 1748-1755.
21. N. Jackson, A. Sridharan, S. Anand, M. Baker, M. Okandan and J. Muthuswamy, *Front Neuroeng*, 2010, **3**, 10.
22. J. Muthuswamy, M. Okandan, A. Gilletti, M. S. Baker and T. Jain, *IEEE Trans Biomed Eng*, 2005, **52**, 1470-1477.